

Main-chain poly(ionic liquid)-derived nitrogen-doped micro/mesoporous carbons for CO₂ capture and selective aerobic oxidation of alcohols

Jiang Gong ^a, Huijuan Lin ^a, Konrad Grygiel ^a, Jiayin Yuan ^{a,b,*}

^a Department of Colloid Chemistry, Max Planck Institute of Colloids and Interfaces, Research Campus Golm, 14476, Potsdam, Germany

^b Department of Chemistry and Biomolecular Science, and Center for Advanced Materials Processing, Clarkson University, 8 Clarkson Avenue, 13699 Potsdam, USA

*Corresponding author. E-mail address: jyuan@clarkson.edu

Abstract: Sustainable development and the recent fast-growing global demands for energy and functional chemicals urgently call for effective methods for CO₂ remediation and efficient metal-free catalysts for selective oxidation of aromatic alcohol. Herein, a unique main-chain poly(ionic liquid) (PIL) is employed as the precursor to prepare nitrogen-doped micro/mesoporous carbons *via* simultaneous carbonization and activation, which bear high yield, large specific surface area above 1700 m² g⁻¹ and rich nitrogen dopant. The porous carbon products deliver a high CO₂ adsorption capacity up to 6.2 mmol g⁻¹ at 273 K and 1 bar with outstanding reversibility and satisfactory selectivity. Besides, they work excellently as metal-free carbocatalysts for the selective aerobic oxidation of benzyl alcohol to benzaldehyde with high selectivity. It is believed that this work not only provides a facile approach to prepare nitrogen-doped porous carbon, but also advances the related research in the fields of environment and catalysis.

Keywords: Nitrogen-doped porous carbon, CO₂ capture, selective aerobic oxidation, metal-free carbocatalyst, poly(ionic liquid)s

1. Introduction

CO₂ emission is an important issue in the establishment of a sustainable modern society and is currently one of the driving forces to implement the green chemistry concept. The accumulation of CO₂ in atmosphere is widely considered as a primary factor in global climate change. Carbon capture and sequestration technologies have been proposed to be one of solutions [1,2]. One of the industrial techniques for CO₂ capture is chemical sorption by aqueous solution of organic amines [3]. Although these systems can achieve a high sorption capacity, they suffer from one or more of the following drawbacks, such as solvent loss, corrosion and high energy consumption for regeneration. There is also huge interest in chemical conversion of CO₂ into industrial raw materials [4]. Recently, significant research efforts have been devoted to exploring porous materials with large specific surface area, *e.g.*, porous frameworks (including metal organic framework (MOF) and zeolitic imidazolate framework (ZIF)) [5-8], zeolites [9], and carbons [10-12]. Nevertheless, developing porous adsorbents that efficiently capture CO₂ and mitigate the dilemma remains a challenging but imperative task. In parallel, the selective aerobic oxidation of aromatic alkanes/alcohols to their corresponding aldehydes/ketones is one of the most important transformations of functional groups in organic synthesis, both for fundamental research and industrial manufacturing [13-15]. Plenty of metal-catalyzed aerobic processes, especially based on noble metals, have been studied [16,17]. Considering the scarcity and high cost of noble metals and the sustainability and rational use of resources, it would be highly desirable to explore metal-free catalysts for these reactions.

Nitrogen-doped porous carbons bearing combined micro/mesopores represent an emerging class of porous materials of versatile functionalities and tunable porosities [18-20]. The micropores in a high density packing deliver a high surface area, therefore abundant active sites for both sorption and catalytic reactions, whereas the mesopores, beside their moderate surface area, enhance mass transport and diffusion of sorbates and reagents [21-23]. Additionally, from the viewpoint of heteroatom doping, the incorporation of nitrogen into graphitic carbon networks improves the oxidation stability and basicity through conjugation between the lone electron pair of nitrogen and the π system of carbon lattice [24]. Owing to

these advantages, nitrogen-doped micro/mesoporous carbons have exhibited potential applications in many fields such as energy [25-27], catalysis [28-30], and environment [31, 32]. In particular, they are promising CO₂ adsorbents thanks to the basic nitrogen sites that improve affinity towards acidic CO₂ molecules [33]. Furthermore, previous study has found that the nitrogen sites of carbocatalysts are pivotal for the C-H bond activation, because nitrogen dopant alters local electronic structure of the adjacent carbon atoms and promotes catalytic reactivity [13]. There have already been some pioneer works in this field [34,35], nevertheless fabricating functional nitrogen-doped porous carbons in replacement of precious metal-based catalysts is actively pursued for green chemical processes.

To synthesize nitrogen-doped porous carbons, a major concern is the choice of precursor, of which the chemical structure affects the production yield, nitrogen content, graphitic structure, *etc.* The yields of common organic carbon precursors are generally below 40 wt % at high temperatures (*e.g.*, 900 °C, see Table S1), as most of organic compounds completely evaporate or decompose during high temperature carbonization. Since the first report on the conversion of poly(ionic liquid)s (PILs) into porous carbon in 2010 [36], PILs have been considered to be an important class of polymer-based carbon precursors. Compared to other polymers [37,38], structurally well-defined PILs are thermally more stable at temperatures up to 400 °C, and they contain rich heteroatoms, nitrogen in most cases, yielding heteroatom-doped carbons in good yield [39,40]. The favorable thermal stability of PILs is related to their ionic nature, aromatic nature as well as some network-forming groups [41], such as cyano group that undergoes trimerization reaction to form polytriazine network under charring conditions [42].

Herein, we report how to synthesize functional porous carbons with an unusually high yield at 900°C (47 wt % to 67 wt % dependent on the activation agent amount) from a main-chain PIL simultaneously bearing nitrogen-rich imidazolium cation, cyano group and aromatic ring *via* one-step carbonization/activation process. The as-formed nitrogen-doped carbons bearing abundant micro/mesopores not only store CO₂ as high as 6.2 mmol g⁻¹ at 273 K and 1 atm but also serve as high-performance metal-free carbocatalysts for selective aerobic oxidations, here exemplified by the conversion of benzyl alcohol to benzaldehyde.

2. Materials and methods

2.1. Materials

Glacial acetic acid (purity $\geq 99.7\%$, Alfa Aesar), *p*-phenylenediamine (purity $\geq 99\%$, Sigma-Aldrich), pyruvaldehyde (40% aqueous solution, Sigma-Aldrich), formaldehyde (37% aqueous solution, Sigma-Aldrich), sodium dicyanamide ($\text{NaN}(\text{CN})_2$, purity $\geq 96\%$, Sigma-Aldrich), potassium hydroxide (KOH, purity $\geq 90\%$, Sigma-Aldrich), and benzyl alcohol (purity $\geq 99\%$, Sigma-Aldrich) were of analytical grade and used as received without further purifications. All other chemicals were utilized without further purifications.

2.2. Synthesis of the PIL precursor (PILPhDCA)

Firstly, an imidazolium-type PILPhAc was synthesized in water *via* one-pot modified Debus-Radziszewski reaction (Scheme 1), as we reported previously [43]. In a typical run, Milli-Q[®] water (400 mL) and glacial acetic acid (33.0 mL) were added under vigorous stirring to 10.0 g of *p*-phenylenediamine. Such mixture was then injected to the mixture of pyruvaldehyde (14.6 mL) and formaldehyde (7.1 mL). The solution was stirred for 15 min, diluted with Milli-Q[®] water and dialyzed against Milli-Q[®] water (the molecular weight cut-off of dialysis bag is 3.5 kDa) for 1 week. PILPhDCA was prepared by anion exchange from PILPhAc with excessive $\text{NaN}(\text{CN})_2$ in aqueous solution. In a typical run, 4.0 g of PILPhAc was added to 800 mL of Milli-Q[®] water. After complete dissolution, 100 mL of an aqueous solution containing 5 molar equivalents of $\text{NaN}(\text{CN})_2$ was added under vigorous stirring for 30 min. The precipitation occurred. The precipitate was filtered off, washed with Milli-Q[®] water several times, and dried at 80 °C to constant weight under high vacuum.

2.3. Preparation of nitrogen-doped porous carbons (NPCs)

Dried PILPhDCA powder was firstly mixed with KOH in Milli-Q[®] water at a KOH/PILPhDCA mass ratio of 2, 4 and 6, respectively. The mixture was agitated for 30 min to achieve a uniform suspension, and then dried at 80 °C to obtain a solid mixture of KOH and PILPhDCA. Afterwards, the solid mixture was heated at 450 °C for 1 h under nitrogen atmosphere and subsequently calcined at 900 °C for 1 h. The ramping rate was maintained at

10 °C min⁻¹ using a Nabertherm N7/H chamber oven with a P300 controller. After slowly cooling down to room temperature, the product was repeatedly washed with 1 mol L⁻¹ HCl and Milli-Q[®] water until the pH value of the filtrate reached 7 ± 0.5 to ensure the efficient removal of KOH (< 0.05 wt% in the final carbon products), and finally dried at 110 °C under vacuum for 12 h. The resultant activated carbon sample was named as NPC-2, NPC-4 and NPC-6, respectively, while the carbon product prepared from merely PILPhDCA in the absence of KOH under the similar preparation process was denoted as NPC-0.

2.4. Characterization

Proton nuclear magnetic resonance (¹H NMR) spectra were recorded at room temperature on a VARIAN 400-MR (400 MHz) spectrometer using DMSO-*d*₆ as the solvent. Attenuated total reflection (ATR) Fourier-transform infrared spectroscopy (FTIR) was performed at room temperature on a BioRad 6000 FT-IR spectrometer equipped with a Single Reflection Diamond ATR. Gel permeation chromatography (GPC) was performed by using NOVEMA-column with a mixture of 80% of acetate buffer and 20% of methanol (flow rate = 1.0 mL min⁻¹, dextran standards using RI detector-RI-101 Refractometer). Thermogravimetric analysis (TGA) experiment was performed under nitrogen flow at a heating rate of 10 °C min⁻¹ using a Netzsch TG209-F1 apparatus. Nitrogen adsorption/desorption experiments were performed with a Quantachrome Autosorb and Quadrasorb at 77 K, and the data were analyzed using Quantachrome software. The specific surface area was calculated using the Brunauer-Emmett-Teller (BET) equation. The samples were degassed at 150 °C for 24 h before measurements. Combustion elemental analyses were done with a varioMicro elemental analysis instrument from Elementar Analysensysteme. The surface element compositions were characterized by means of X-ray photoelectron spectroscopy (XPS) carried out on a VG ESCALAB MK II spectrometer using an Al K α exciting radiation from an X-ray source operated at 10.0 kV and 10 mA. Scanning electron microscopy (SEM) measurements were carried out in a LEO 1550-Gemini electron microscope (acceleration voltage = 3 kV), and the samples were coated with a thin gold layer before SEM measurements. Energy-dispersive X-ray (EDX) map was taken on the SEM with

an EDX spectrometer. Transmission electron microscopy (TEM) measurements were performed using a Zeiss EM 912 (acceleration voltage = 120 kV). High-resolution TEM (HRTEM) measurement was carried out on a FEI Tecnai G2 S-Twin transmission electron microscope operating at 200 kV. X-ray diffraction (XRD) pattern was recorded on a Bruker D8 diffractometer using Cu K α radiation ($\lambda = 0.154$ nm) and a scintillation counter. Raman spectrum was collected using a confocal Raman microscope ($\alpha 300$; WITec, Ulm, Germany) equipped with a 532 nm laser. Gas chromatography-mass spectrometry (GC-MS) analyses were performed using an Agilent Technologies 5975 gas chromatograph equipped with a MS detector and a capillary column (HP-5MS, 30 m \times 0.25 mm \times 0.25 μ m). The temperature program started with an isothermal step at 50 $^{\circ}$ C for 2 min, in a second step the temperature was increased to 300 $^{\circ}$ C at a rate of 30 $^{\circ}$ C min $^{-1}$ and then kept for 1 min.

2.5. CO $_2$ capture

CO $_2$ capture by NPCs was conducted by measuring the adsorption isotherms at 0 and 25 $^{\circ}$ C in a Quantachrome Autosorb and Quadrasorb (Quantachrome Instruments). NPCs were firstly degassed at 150 $^{\circ}$ C for 30 h before each analysis. The isosteric heat of adsorption (Q_{st}) was calculated by applying the Clausius-Clapeyron equation to the adsorption isotherms measured at the aforementioned two temperatures:

$$\ln\left(\frac{p_1}{p_2}\right) = Q_{st} \times \frac{T_2 - T_1}{R \times T_1 \times T_2} \quad (1)$$

where R is the universal gas constant (8.314 J mol $^{-1}$ K $^{-1}$), p_1 and p_2 denote the pressure (Pa), and T_1 and T_2 represent the absolute temperature (K).

The breakthrough experiment of NPC-4 was performed in a small-scale fixed-bed column. The feed stream with a composition of CO $_2$ /N $_2$ (20% of CO $_2$ in volume) was fed into the column at a flow rate of 20 mL min $^{-1}$. Prior to the sorption experiment, the sample was heated to 200 $^{\circ}$ C under N $_2$ flow at 100 mL min $^{-1}$ for 2 h to desorb adventitious CO $_2$ and water, slowly cooled to 25 $^{\circ}$ C and then exposed to CO $_2$ for the experimental sorption run.

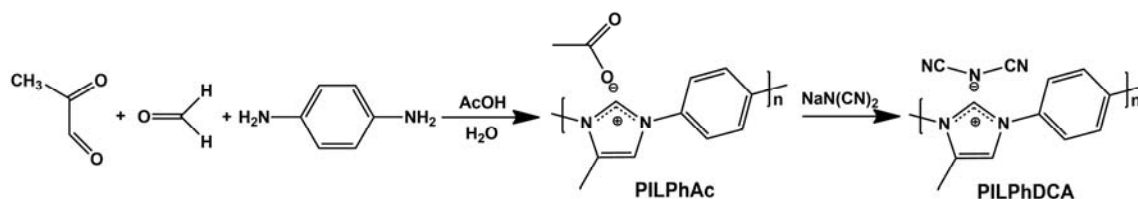
2.6. Selective aerobic oxidation of benzyl alcohol

The aerobic oxidation reaction was carried out in Schlenk tube containing 40 mg of catalyst (optimized amount), 100 mg of benzyl alcohol, and a stir bar at 60 (or 100) °C under a static O₂ atmosphere (1 atm). After the reaction was completed, the reaction mixture was centrifuged at 8000 rpm for 2 min to separate the catalyst for the later analyses of GC-MS and ¹H NMR.

3. Results and discussion

3.1. Synthesis and characterization of the PIL precursor

The synthetic route to the main-chain PILPhDCA is depicted in Scheme 1, based on our recent work [43]. An imidazolium-type PILPhAc was firstly synthesized *via* one-pot modified Debus-Radziszewski reaction in water at room temperature. Briefly, water and glacial acetic acid were added to *p*-phenylenediamine under vigorous stirring. The solution was injected to a mixture of pyruvaldehyde and formaldehyde to prepare PILPhAc. PILPhDCA was obtained by anion exchange of PILPhAc with excessive NaN(CN)₂ in aqueous solution. The successful synthesis of PILPhDCA is verified by ¹H NMR, FTIR, and GPC measurements (Figs. S1–S3).



Scheme 1 Schematic illustration of the PILPhDCA synthesis *via* one-pot modified Debus-Radziszewski reaction in water at room temperature.

The thermal stability of PILPhDCA was studied by TGA under nitrogen atmosphere (Figs. 1 and S4). The temperature at the maximum weight loss rate ranges from 360 to 510 °C, which is mainly attributed to the fractionation during the crosslinking reaction of the cyano group [43]. Surprisingly, the carbonization yields at 600 and 900 °C according to the TGA analysis are 73 and 66 wt %, respectively. The unusually high carbonization yield of PILPhDCA is attributed to its special chemical structure bearing both cyano group to form

stable networks and aromatic backbone systems that end up in the final carbon product with less weight loss.

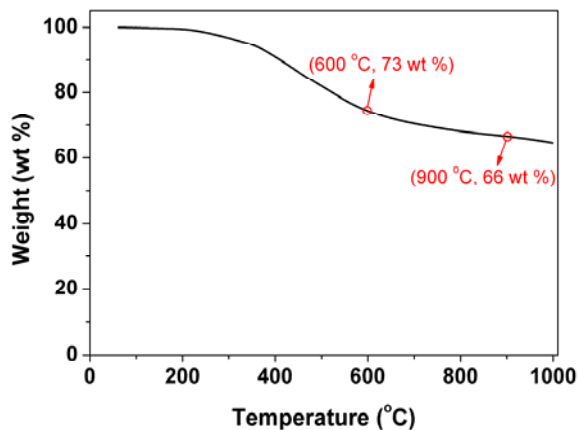


Fig. 1. TGA curve of PILPhDCA under nitrogen atmosphere at 10 °C min⁻¹.

It is well known that ionic liquid and PIL are not volatile, but at elevated temperatures they decompose partially into volatile products. As a result, during heating up to 900 °C under inert gas atmosphere, most PILs decompose nearly completely or leave a small amount of residual mass up to 40 wt % [31,42]. The results above highlight the excellent carbonization function of PILPhDCA as a new precursor for the preparation of nitrogen-doped carbon, which is superior to many common nitrogen-containing polymers (Table S1), *e.g.*, polyaniline [44] and polyacrylonitrile [45].

3.2. Yield, textural property, and element composition of NPCs

Considering the fascinating carbonization yield of PILPhDCA in a bulk state, we modified the carbonization process by adding KOH as activation agent to PILPhDCA at a KOH/PILPhDCA mass ratio of 2, 4 and 6 to prepare nitrogen-doped porous carbons (NPCs). The as-synthesized carbon products after thorough water rinsing are denoted as NPC-2, NPC-4 and NPC-6, respectively, while NPC-0 denotes carbon prepared without KOH. Table 1 presents the yield of NPCs obtained at different KOH/PILPhDCA mass ratios. NPC-0 shows an ultrahigh yield of 67 wt % at 900 °C, which is in good agreement with the TGA result (66 wt % in Fig. 1). When the KOH/PILPhDCA mass ratio increases to 2, the resultant

NPC-2 still exhibits a high yield of 58 wt %. The decrease in carbonization yield is attributed to the etching of the as-formed graphitic layers by KOH at the carbonization temperature to generate porous structure, which will be clarified in detail in the following part. Further increasing KOH/PILPhDCA mass ratio leads to a gradual decrease in the carbonization yield of NPCs, e.g., 54 wt % for NPC-4 and 47 wt % for NPC-6. Nevertheless they are significantly high in comparison to many polymeric precursors. The superior carbonization yield and easy implementation enable a large-scale production of NPCs, for example in a 40 g scale (Fig. S5), the largest capacity allowed by our laboratory carbonization oven.

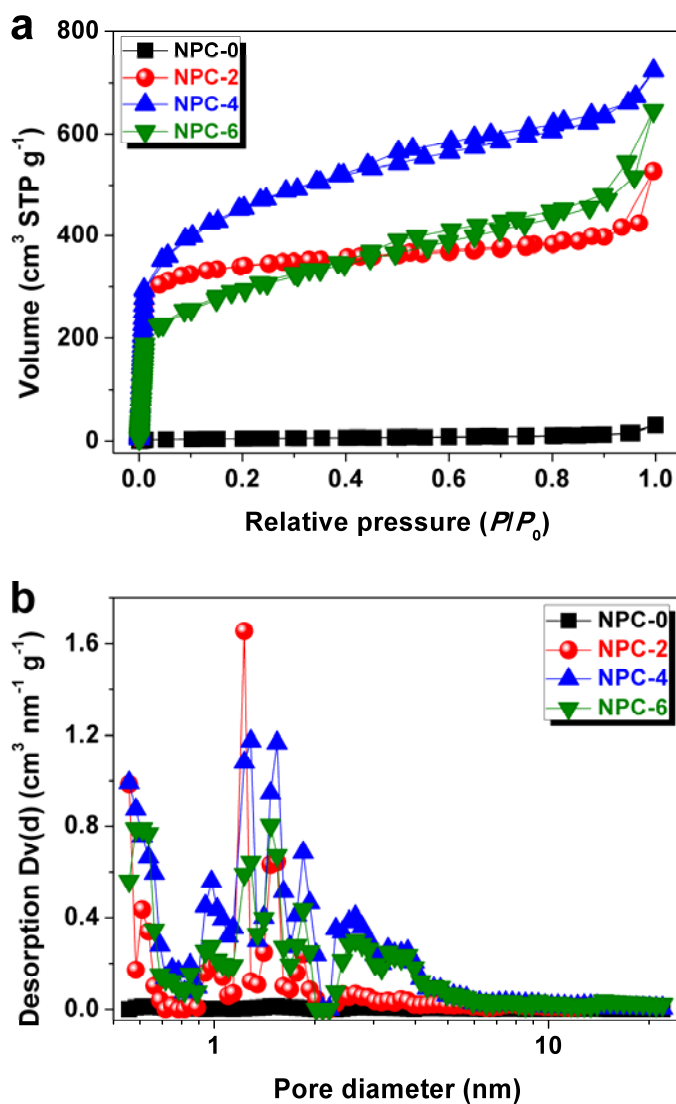


Fig. 2. (a) Nitrogen adsorption/desorption isotherms at 77 K and (b) pore size distribution plots of NPCs prepared at different KOH/PILPhDCA mass ratios.

The porosity of carbon materials was probed using nitrogen gas sorption at 77 K. Fig. 2 shows the nitrogen adsorption/desorption isotherms and pore size distribution plots of the as-prepared NPCs. NPC-0 displays a negligible specific surface area (S_{total}) of $17 \text{ m}^2 \text{ g}^{-1}$ and low pore volume (V_{total}) of $0.024 \text{ cm}^3 \text{ g}^{-1}$ (Table 1), that is to say, a poorly porous carbon. In comparison, the nitrogen adsorption/desorption isotherms of NPC-2 exhibit type I isotherm with a significant adsorption at the relative pressure $P/P_0 < 0.1$ due to the capillary filling of micropores, revealing the presence of rich micropores. The S_{total} and V_{total} of NPC-2 are determined to be $1216 \text{ m}^2 \text{ g}^{-1}$ and $0.963 \text{ cm}^3 \text{ g}^{-1}$, respectively. Compared with NPC-0, the substantial S_{total} and V_{total} enhancements of NPC-2 are obviously attributed to KOH activation. The activation mechanism is normally suggested to be the following reaction [46]:



When the temperature is higher than $700 \text{ }^\circ\text{C}$, the reaction proceeds as follows:



When the temperature is higher than $800 \text{ }^\circ\text{C}$, it can be expressed as:



With the increase of KOH/PILPhDCA mass ratio, the obtained NPC-4 and NPC-6 display type I/IV isotherms. A higher adsorption capacity is observed at the low relative pressure $P/P_0 < 0.1$, meaning the presence of more micropores. Besides, a detectable type-H4 hysteresis loop at the relative pressure P/P_0 ranging from 0.4 to 0.8 is found, corresponding to the filling and emptying of mesopores by capillary condensation. This result implies that the addition of more KOH is propitious to the formation of both micropores and mesopores. NPC-4 thus exhibits the highest S_{total} ($1742 \text{ m}^2 \text{ g}^{-1}$) and largest V_{total} ($1.415 \text{ cm}^3 \text{ g}^{-1}$). After further increasing the amount of KOH, the micropores are prone to merge into mesopores and/or macropores; NPC-6 thereupon displays relatively lower S_{total} ($1141 \text{ m}^2 \text{ g}^{-1}$) and V_{total} ($1.063 \text{ cm}^3 \text{ g}^{-1}$) than NPC-4, but still higher than NPC-0.

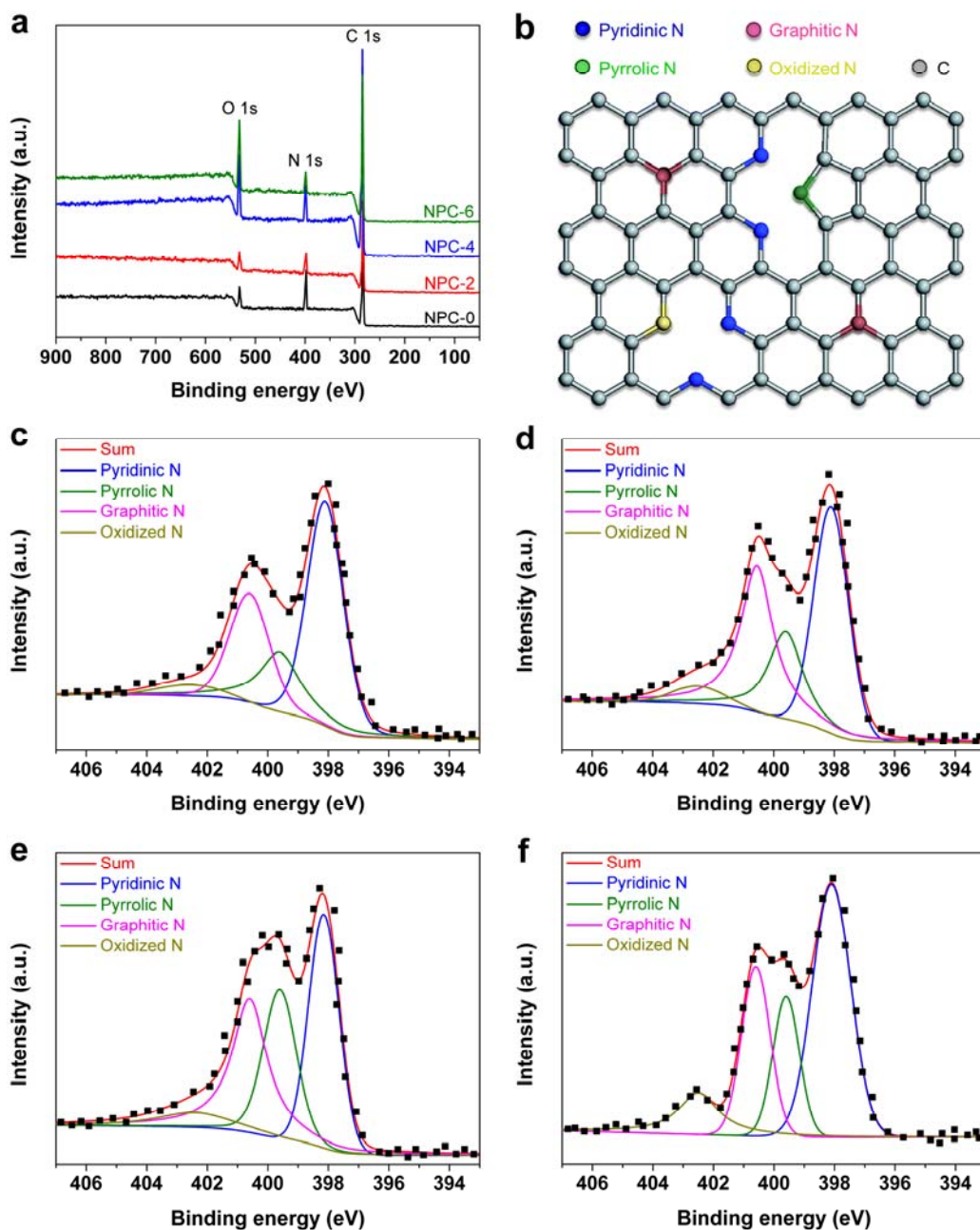


Fig. 3. (a) XPS spectra of NPCs, (b) scheme of nitrogen element with different states, and high-resolution N 1s XPS spectra of (c) NPC-0, (d) NPC-2, (e) NPC-4, and (f) NPC-6.

Combustion element analyses were carried out to access the element compositions of NPCs (Table S2). Generally, they consist of carbon (79.6–82.0 wt %), nitrogen (3.7–10.7 wt %) and oxygen (7.0–14.9 wt %) with a trace amount of hydrogen (1.6–2.0 wt %). Upon the increase of KOH/PILPhDCA mass ratio, the nitrogen content decreases while oxygen

content increases, which are consistent with the previous study [47]. The surface element compositions of NPCs were investigated by using XPS. The full XPS survey spectra of NPCs show the expected presences of carbon, nitrogen and oxygen (Fig. 3a). Their compositions were calculated from the corresponding peak areas of XPS spectra (Table S3). Curve deconvolution shows that the high-resolution N 1s spectra of the samples can be well-fitted to the superposition of four peaks. The peaks with binding energies centered at 398.4, 400.4, 401.3 and 404.6 eV are assigned to pyridinic, pyrrolic, graphitic and oxidized N, respectively (Fig. 3b). Pyridinic N and graphitic N are the dominant nitrogen-containing surface functional groups in all samples, with the contents in the ranges of 33.7–48.2% and 23.8–35.8%, respectively (Figs. 3c–3f, Table S3). Pyrrolic N and oxidized N cannot be neglected, with the abundance in the range of 17.8–25.4% and 4.5–12.2%, respectively.

3.3. Morphology, microstructure, and phase structure of NPCs

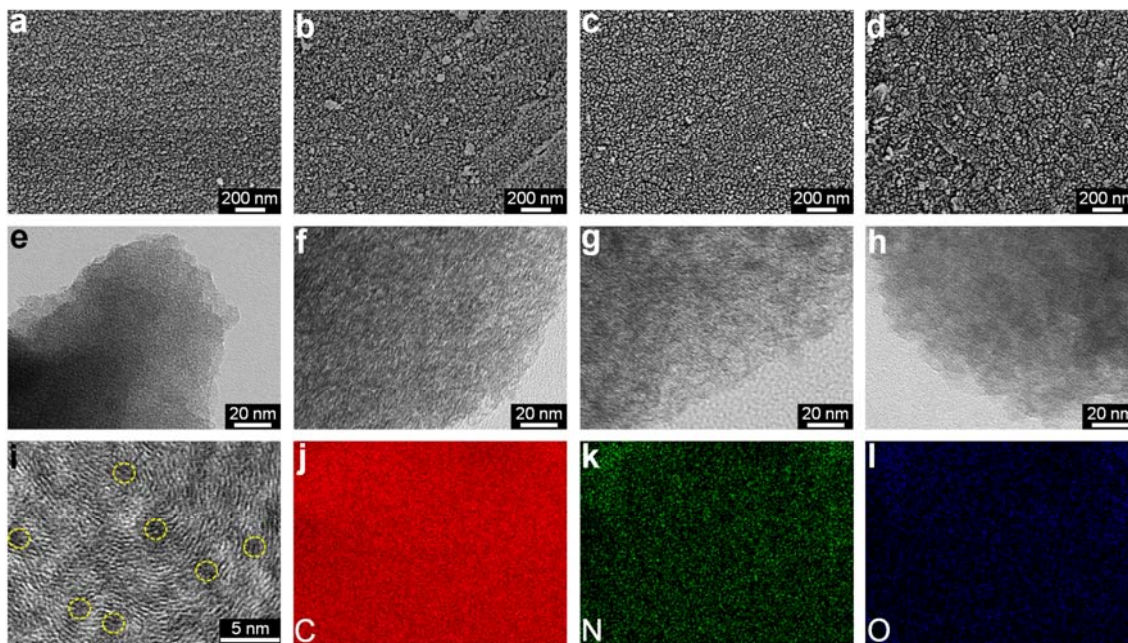


Fig. 4. SEM images of (a) NPC-0, (b) NPC-2, (c) NPC-4 and (d) NPC-6 with a high magnification. TEM images of (e) NPC-0, (f) NPC-2, (g) NPC-4 and (h) NPC-6. (i) HRTEM image of NPC-4; the yellow cycles show the nanoscale pores. EDX maps of (j) carbon, (k) nitrogen, and (l) oxygen for NPC-4 according to SEM image (c).

Fig. 4 displays SEM and TEM images of typical areas of the NPC-*x* samples. With the mass ratio of KOH to PILPhDCA increasing from 0 to 6, the bulk morphologies of NPCs display no obvious differences (Fig. S6), being composed of dense patch-like particles with a size ranging from 10 to 40 nm (Figs. 4a–4d). To observe the local microstructure of NPCs, TEM characterization was carried out. A large number of nanopores are found in NPCs except NPC-0 (Figs. 4e–4h). HRTEM was conducted to observe the subnanometer structure of the NPC-4 product (Fig. 4i). The dark patterns are stacked bent graphitic layers in a nanoscale size, indicating a short-range order of graphitic crystallite. Pores of few nanometers (pointed by cycles) were also observed in the NPC-4, similar to the porous graphene activated by KOH as reported previously [48]. EDX maps of carbon, nitrogen and oxygen (Figs. 4j–4l) certify that the NPC-4 sample is uniform with respect to element distributions.

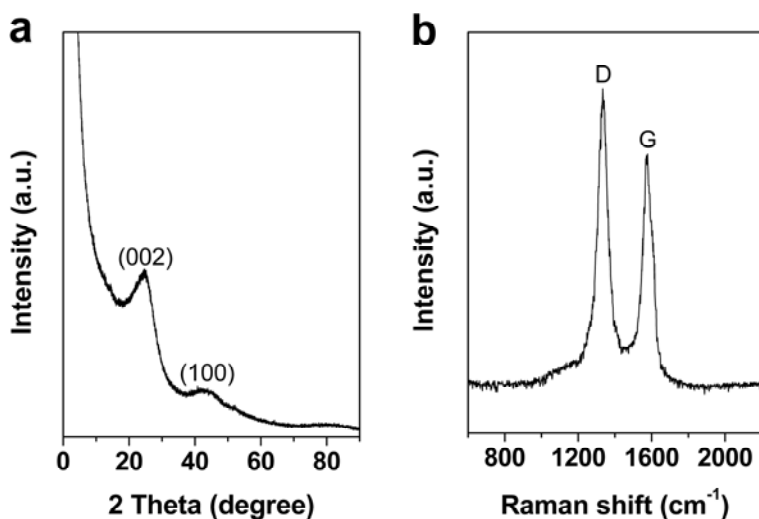


Fig. 5. (a) XRD pattern and (b) Raman spectrum of NPC-4.

To investigate the phase structure of NPCs, XRD characterization was employed (Fig. 5a). The appearances of two broad diffraction peaks at $2\theta = 25^\circ$ and 42° , which are assigned to the typical graphitic (002) and (100) planes, respectively, reveal the turbostratic structure of NPC-4. Raman spectroscopy was used to gain more insights into the phase structure information of NPC-4 (Fig. 5b). The D band at $\sim 1333\text{ cm}^{-1}$ and G band at $\sim 1578\text{ cm}^{-1}$ are related to the disordered and defective structure of carbon and the ordered carbon structure with sp^2 electronic configuration, respectively [49]. The relatively low I_G/I_D value (~ 0.61)

indicates the partial graphitization of NPC-4, typical for microporous carbons, which is caused by the defects generated by both nitrogen doping and KOH activation.

3.4. CO₂ capture by NPCs

The CO₂ adsorption isotherms of the as-prepared NPCs are shown in Fig. 6a. In spite of rather low specific surface area (17 m² g⁻¹), NPC-0 exhibits a moderate CO₂ uptake of 2.0 mmol g⁻¹ at 273 K and 1 bar. This is no doubt due to the incorporation of abundant nitrogen functionalities (10.7 wt %), which act as basic sites for fastening acidic CO₂ molecules. The CO₂ adsorption capacity dramatically grows up to 5.0 mmol g⁻¹ for NPC-2 and 6.2 mmol g⁻¹ for NPC-4, and then declines to 4.3 mmol g⁻¹ for NPC-6. The ultra-high specific surface area, large pore volume (particularly the narrow micropores *via* pore filling mechanism) and rich nitrogen dopants (especially the pyridinic N and pyrrolic N due to acid-base interaction) of NPC-2 and NPC-4 mainly contribute to the significant improvement of CO₂ uptake. The decreasing CO₂ uptake by NPC-6 in comparison to NPC-2 and NPC-4 is reasonable because of the decreased specific surface area and nitrogen dopant. Moreover, the CO₂ uptake by NPC-4 at 298 K and 1 bar is measured to be 4.5 mmol g⁻¹, which is 19.8 wt % of the porous carbon (Fig. 6b). These results are among the top values reported for porous adsorbents [33,37,50-65] (see Table 2).

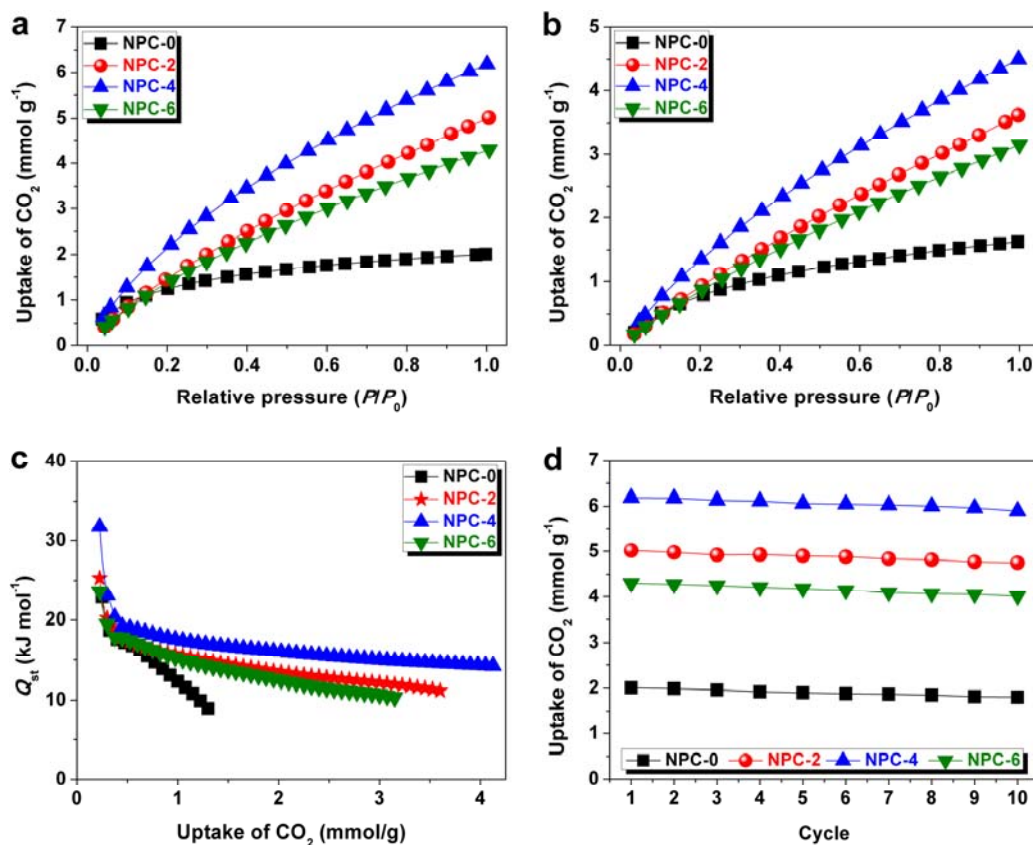


Fig. 6. CO₂ adsorption isotherms of NPCs measured at (a) 273 K and (b) 298 K. (c) Isothermic heats of CO₂ adsorption for NPCs at different CO₂ uptake amounts. (d) The reusability of NPCs for CO₂ uptake over 10 cycles at 273 K.

Under similar experimental conditions, the N₂ adsorption capacity of NPC-4 is measured to be 0.45 and 0.35 mmol g⁻¹ in maximum at 273 and 298 K, respectively (Fig. S7), which are considerably lower than that for CO₂. The initial slopes of CO₂ and N₂ adsorption isotherms are calculated, and the ratio of these slopes is applied to estimate the adsorption selectivity for CO₂ over N₂. As a result, the apparent CO₂/N₂ selectivity of NPC-4 at 273 and 298 K is determined to be 14 and 17, respectively, indicating that NPC-4 could be a potential selective adsorbent for CO₂/N₂ separation. Additionally, by fitting the CO₂ adsorption isotherms of NPCs at 273 and 298 K, the isothermic heats of CO₂ adsorption (Q_{st}) are calculated by using Clausius-Clapeyron equation. The calculated Q_{st} values (Fig. 6c) are in the ranges of 8–23 kJ mol⁻¹ for NPC-0, 11–25 kJ mol⁻¹ for NPC-2, 15–32 kJ mol⁻¹ for NPC-4, and 10–24 kJ mol⁻¹ for NPC-6, depending on different CO₂ uptake amounts. Evidently,

NPC-4 shows higher Q_{st} than other NPCs. These values are comparable to, if not higher than those of the previously reported adsorbents [62,63], which is probably owing to the significant presence of micropores and the strong interaction between basic nitrogen species and acidic CO₂ molecules. Furthermore, the reusability of NPCs for CO₂ capture at 273 K is tested over 10 cycles (Fig. 6d). The CO₂ adsorption capacity of NPC-4 after 10 cycles retains up to 5.9 mmol g⁻¹, higher than that of other NPCs, which indicates the good recyclability of NPC-4 for CO₂ capture.

To assess the potential of the sorbent in practical processes, more realistic conditions are required, *i.e.*, competitive CO₂ adsorption with N₂ in a dynamic system (Fig. S8). In a typical experiment, a mixed gas stream of 20% (v/v) CO₂ + 80% (v/v) N₂ was used to approximately simulate a postcombustion flue gas. At 298 K and 0.2 bar partial pressure of CO₂, the dynamic CO₂ capacity of NPC-4 is 1.25 mmol g⁻¹, which matches with that from the equilibrium measurement using pure CO₂ at 298 K and 0.2 bar, *i.e.*, 1.35 mmol g⁻¹. This implies that CO₂ preferentially adsorbs onto the sorbent over N₂, even in a CO₂/N₂ mixture.

3.5. Selective aerobic oxidation of benzyl alcohol to benzaldehyde by NPCs

It is widely acknowledged that the nitrogen dopant promotes the catalytic reactivity of carbocatalysts *via* altering the electronic structure of the adjacent carbon atoms, meanwhile the mesopores enhance the mass transport and diffusion of reagents. Consequently, nitrogen-doped micro/mesoporous carbons can be potential metal-free carbocatalysts for selective aerobic oxidations, and replace conventional base, metal and metal oxide catalysts. Here, to exemplify the application of NPCs as metal-free carbocatalysts, the selective aerobic oxidation of benzyl alcohol to higher value-added product benzaldehyde is conducted as a model reaction. Benzaldehyde has tremendous applications in perfumery, pharmaceutical, dyestuff and agrochemical industries. Commercially, benzaldehyde is synthesized by the hydrolysis of benzyl chloride or the vapor/liquid-phase oxidation of toluene. However, in the former process, traces of chlorine inevitably exist in the product benzaldehyde, while in the latter case, the selectivity to benzaldehyde is very poor.

Table 3 lists the activity results obtained with a range of reaction conditions. As the

reaction temperature increases from 60 to 100 °C, the conversion of benzyl alcohol catalyzed by NPC-4 after 24 h grows up from 58.8% to 99.5%, while the selectivity keeps at 100% (entries 1 and 2). When the reaction time decreases from 24 to 12 h, a high benzyl alcohol conversion of 73.1% is retained with a selectivity of 100% (entry 3). In the control experiment using NPC-0 as catalyst, a negligible amount (0.5%) of benzyl alcohol is selectively oxidized to benzaldehyde after 24 h (entry 4), implying that apart from nitrogen dopant, the pore architecture is crucial for determining the catalytic performance. Previous report demonstrates that the sorption and activation of molecular oxygen over the graphitic nitrogen active sites to form a sp^2 N-O₂ adduct transition state is a key step [66]. Here, the high specific surface area and large pore volume of NPC-4 facilitate the easy accessibility of these active sites by molecular oxygen and benzyl alcohol, thus being beneficial for their sorption and mass transport in catalytic reaction. As an additional proof, in the control experiments using NPC-2 and NPC-6 as carbocatalysts (entries 5 and 6), the conversion of benzyl alcohol is 93.2% and 87.5%, respectively, which is lower than NPC-4 but apparently far beyond NPC-0.

To evaluate the reusability, the used NPC-4 was separated by centrifuge after the first oxidation run and employed for the next run under the same condition. After three runs (entries 7 and 8), the decreases of alcohol conversion and selectivity are negligible, suggesting the good reusability of NPC-4. It is worth pointing out that NPC-4 prevails over the previous catalysts (entries 9–14), including N-doped graphene [14], P-doped porous carbon [67], graphene oxide [68], N/O/S-doped porous carbon [69], and carbon nitride [15].

4. Conclusions

In summary, a novel main-chain poly(ionic liquid) bearing both cyano group and aromatic backbone conjugates have been applied as nitrogen-rich carbon precursor with unusually high carbonization yield at 900 °C (47 wt % to 67 wt %). Through simultaneous carbonization and activation of the poly(ionic liquid), nitrogen-doped micro/mesoporous carbons were prepared, which display large specific surface area up to 1742 m² g⁻¹ and rich nitrogen dopant. They deliver an unprecedented high CO₂ uptake with satisfactory selectivity and outstanding

reversibility. Equally important, they serve excellently as metal-free carbocatalysts for the selective aerobic oxidation of benzyl alcohol to benzaldehyde with high conversion and selectivity. We believe that this work not only opens up a new avenue to synthesize appealing heteroatom-doped porous carbons in a high yield by rational architecture design of the polymeric precursor, but also greatly advances the related research in the fields of environment remediation and heterogeneous catalysis.

Acknowledgements

This work was supported by the Max Planck Society for financial support. J.G. thanks Prof. Tao Tang for XPS measurements and Mr. Max Braun for GC-MS measurements. J.Y. and J.G. thank the financial support from the European Research Council (ERC) Starting Grant with project number 639720–NAPOLI.

References

- [1] Q. Yang, Z. Wang, Z. Bao, Z. Zhang, Y. Yang, Q. Ren, H. Xing, S. Dai, New insights into CO₂ absorption mechanisms with amino-acid ionic liquids, *ChemSusChem* 9 (2016) 806-812.
- [2] Q. Chen, M. Luo, P. Hammershøj, D. Zhou, Y. Han, B.W. Laursen, C.-G. Yan, B.-H. Han, Microporous polycarbazole with high specific surface area for gas storage and separation, *J. Am. Chem. Soc.* 134 (2012) 6084-6087.
- [3] D.M. D'Alessandro, B. Smit, J.R. Long, Carbon dioxide capture: Prospects for new materials, *Angew. Chem. Int. Ed.* 49 (2010) 6058-6082.
- [4] R. Arrigo, M.E. Schuster, S. Wrabetz, F. Girgsdies, J.-P. Tessonnier, G. Centi, S. Perathoner, D.S. Su, R. Schlögl, New insights from microcalorimetry on the FeO_x/CNT-based electrocatalysts active in the conversion of CO₂ to fuels, *ChemSusChem* 5 (2012) 577-586.
- [5] W.M. Verdegaal, K. Wang, J.P. Sculley, M. Wriedt, H.-C. Zhou, Evaluation of metal-organic frameworks and porous polymer networks for CO₂-capture applications, *ChemSusChem* 9 (2016) 636-643.
- [6] R.T. Woodward, L.A. Stevens, R. Dawson, M. Vijayaraghavan, T. Hasell, I.P. Silverwood, A.V. Ewing, T. Ratvijitvech, J.D. Exley, S.Y. Chong, F. Blanc, D.J. Adams, S.G. Kazarian,

C.E. Snape, T.C. Drage, A.I. Cooper, Swellable, water- and acid-tolerant polymer sponges for chemoselective carbon dioxide capture, *J. Am. Chem. Soc.* 136 (2014) 9028-9035.

[7] Z. Xiang, R. Mercado, J.M. Huck, H. Wang, Z. Guo, W. Wang, D. Cao, M. Haranczyk, B. Smit, Systematic tuning and multifunctionalization of covalent organic polymers for enhanced carbon capture, *J. Am. Chem. Soc.* 137 (2015) 13301-13307.

[8] H. Furukawa, K.E. Cordova, M.O. Keeffe, O.M. Yaghi, The chemistry and applications of metal-organic frameworks, *Science* 341 (2013) 6149-6160.

[9] J.C. Hicks, J.H. Drese, D.J. Fauth, M.L. Gray, G. Qi, C.W. Jones, Designing adsorbents for CO₂ capture from flue gas-hyperbranched aminosilicas capable of capturing CO₂ reversibly, *J. Am. Chem. Soc.* 130 (2008) 2902-2903.

[10] J. Gong, B. Michalkiewicz, X. Chen, E. Mijowska, J. Liu, Z. Jiang, X. Wen, T. Tang, Sustainable conversion of mixed plastics into porous carbon nanosheet with high performances in uptake of carbon dioxide and storage of hydrogen, *ACS Sustain. Chem. Eng.* 2 (2014) 2837-2844.

[11] H. Seema, K.C. Kemp, N.H. Le, S.-W. Park, V. Chandra, J.W. Lee, K.S. Kim, Highly selective CO₂ capture by S-doped microporous carbon materials, *Carbon* 66 (2014) 320-326.

[12] S. Gu, J. He, Y. Zhu, Z. Wang, D. Chen, G. Yu, C. Pan, J. Guan, K. Tao, Facile carbonization of microporous organic polymers into hierarchically porous carbons targeted for effective CO₂ uptake at low pressures, *ACS Appl. Mater. Interfaces* 8 (2016) 18383-18392.

[13] Y. Gao, G. Hu, J. Zhong, Z. Shi, Y. Zhu, D.S. Su, J. Wang, X. Bao, D. Ma, Nitrogen-doped sp²-hybridized carbon as a superior catalyst for selective oxidation, *Angew. Chem. Int. Ed.* 52 (2013) 2109-2113.

[14] J. Long, X. Xie, J. Xu, Q. Gu, L. Chen, X. Wang, Nitrogen-doped graphene nanosheets as metal-free catalysts for aerobic selective oxidation of benzylic alcohols, *ACS Catal.* 2 (2012) 622-631.

[15] F. Su, S.C. Mathew, G. Lipner, X. Fu, M. Antonietti, S. Blechert, X. Wang, mpg-C₃N₄-catalyzed selective oxidation of alcohols using O₂ and visible light, *J. Am. Chem. Soc.* 132 (2010) 16299-16301.

- [16] S. Wang, W.-C. Li, G.-P. Hao, Y. Hao, Q. Sun, X.-Q. Zhang, A.-H. Lu, Temperature-programmed precise control over the sizes of carbon nanospheres based on benzoxazine chemistry, *J. Am. Chem. Soc.* 133 (2011) 15304-15307.
- [17] C.W. Anson, S. Ghosh, S. Hammes-Schiffer, S.S. Stahl, Co(salophen)-catalyzed aerobic oxidation of *p*-hydroquinone: Mechanism and implications for aerobic oxidation catalysis, *J. Am. Chem. Soc.* 138 (2016) 4186-4193.
- [18] J.W.F. To, J. He, J. Mei, R. Haghpanah, Z. Chen, T. Kurosawa, S. Chen, W.-G. Bae, L. Pan, J.B.-H. Tok, J. Wilcox, Z. Bao, Hierarchical N-doped carbon as CO₂ adsorbent with high CO₂ selectivity from rationally designed polypyrrole precursor, *J. Am. Chem. Soc.* 138 (2016) 1001-1009.
- [19] S. Zhang, K. Dokko, M. Watanabe, Direct synthesis of nitrogen-doped carbon materials from protic ionic liquids and protic salts: Structural and physicochemical correlations between precursor and carbon, *Chem. Mater.* 26 (2014) 2915-2926.
- [20] D. Wu, Z. Li, M. Zhong, T. Kowalewski, K. Matyjaszewski, Templated synthesis of nitrogen-enriched nanoporous carbon materials from porogenic organic precursors prepared by ATRP, *Angew. Chem. Int. Ed.* 53 (2014) 3957-3960.
- [21] P. Adelhelm, Y.-S. Hu, L. Chuenchom, M. Antonietti, B.M. Smarsly, J. Maier, Generation of hierarchical meso- and macroporous carbon from mesophase pitch by spinodal decomposition using polymer templates, *Adv. Mater.* 19 (2007) 4012-4017.
- [22] B. Jache, C. Neumann, J. Becker, B.M. Smarsly, P. Adelhelm, Towards commercial products by nanocasting: Characterization and lithium insertion properties of carbons with a macroporous, interconnected pore structure, *J. Mater. Chem.* 22 (2012) 10787-10794.
- [23] D. Zhou, Y. Cui, P.-W. Xiao, M.-Y. Jiang, B.-H. Han, A general and scalable synthesis approach to porous graphene, *Nat. Commun.* 5 (2014) 4716.
- [24] N. Balahmar, A.C. Mitchell, R. Mokaya, Generalized mechanochemical synthesis of biomass-derived sustainable carbons for high performance CO₂ storage, *Adv. Energy Mater.* 5 (2015) 1500867.
- [25] J. Zhang, L. Qu, G. Shi, J. Liu, J. Chen, L. Dai, N,P-codoped carbon networks as efficient metal-free bifunctional catalysts for oxygen reduction and hydrogen evolution

- reactions, *Angew. Chem. Int. Ed.* 128 (2015) 2270-2274.
- [26] L.-F. Chen, Z.-H. Huang, H.-W. Liang, W.-T. Yao, Z.-Y. Yu, S.-H. Yu, Flexible all-solid-state high-power supercapacitor fabricated with nitrogen-doped carbon nanofiber electrode material derived from bacterial cellulose, *Energy Environ. Sci.* 6 (2013) 3331-3338.
- [27] Y. Liang, L. Cai, L. Chen, X. Lin, R. Fu, M. Zhang, D. Wu, Silica nanonetwork confined in nitrogen-doped ordered mesoporous carbon framework for high-performance lithium-ion battery anodes, *Nanoscale* 7 (2015) 3971-3975.
- [28] H.-W. Liang, W. Wei, Z.-S. Wu, X. Feng, K. Müllen, Mesoporous metal-nitrogen-doped carbon electrocatalysts for highly efficient oxygen reduction reaction, *J. Am. Chem. Soc.* 135 (2013) 16002-16005.
- [29] T.V. Vineesh, M.A. Nazrulla, S. Krishnamoorthy, T.N. Narayanan, S. Alwarappan, Synergistic effects of dopants on the spin density of catalytic active centres of N-doped fluorinated graphene for oxygen reduction reaction, *Appl. Mater. Today* 1 (2015) 74-79.
- [30] L. Wang, M. Pumera, Electrochemical catalysis at low dimensional carbons: Graphene, carbon nanotubes and beyond-a review, *Appl. Mater. Today* 5 (2016) 134-141.
- [31] J.P. Paraknowitsch, J. Zhang, D. Su, A. Thomas, M. Antonietti, Ionic liquids as precursors for nitrogen-doped graphitic carbon, *Adv. Mater.* 22 (2010) 87-92.
- [32] S. Zhang, M.S. Miran, A. Ikoma, K. Dokko, M. Watanabe, Protic ionic liquids and salts as versatile carbon precursors, *J. Am. Chem. Soc.* 136 (2014) 1690-1693.
- [33] J. Wei, D. Zhou, Z. Sun, Y. Deng, Y. Xia, D. Zhao, A controllable synthesis of rich nitrogen-doped ordered mesoporous carbon for CO₂ capture and supercapacitors, *Adv. Funct. Mater.* 23 (2013) 2322-2328.
- [34] X. Wang, Y. Li, Nanoporous carbons derived from MOFs as metal-free catalysts for selective aerobic oxidations, *J. Mater. Chem. A* 4 (2016) 5247-5257.
- [35] H. Watanabe, S. Asano, S.-i. Fujita, H. Yoshida, M. Arai, Nitrogen-doped, metal-free activated carbon catalysts for aerobic oxidation of alcohols, *ACS Catal.* 5 (2015) 2886-2894.
- [36] J. Yuan, C. Giordano, M. Antonietti, Ionic liquid monomers and polymers as precursors of highly conductive, mesoporous, graphitic carbon nanostructures, *Chem. Mater.* 22 (2010) 5003-5012.

- [37] M. Sevilla, P. Valle-Vigón, A.B. Fuertes, N-doped polypyrrole-based porous carbons for CO₂ capture, *Adv. Funct. Mater.* 21 (2011) 2781-2787.
- [38] B. Ashourirad, A.K. Sekizkardes, S. Altarawneh, H.M. El-Kaderi, Exceptional gas adsorption properties by nitrogen-doped porous carbons derived from benzimidazole-linked polymers, *Chem. Mater.* 27 (2015) 1349-1358.
- [39] J. Gong, H. Lin, M. Antonietti, J. Yuan, Nitrogen-doped porous carbon nanosheets derived from poly(ionic liquid): Hierarchical pore structures for efficient CO₂ capture and dye removal, *J. Mater. Chem. A* 4 (2016) 7313-7321.
- [40] T.-P. Fellingner, A. Thomas, J. Yuan, M. Antonietti, "Cooking carbon with salt": Carbon materials and carbonaceous frameworks from ionic liquids and poly(ionic liquid)s, *Adv. Mater.* 25 (2013) 5838-5855.
- [41] J.S. Lee, X. Wang, H. Luo, S. Dai, Fluidic carbon precursors for formation of functional carbon under ambient pressure based on ionic liquids, *Adv. Mater.* 22 (2010) 1004-1007.
- [42] Q. Zhao, T.-P. Fellingner, M. Antonietti, J. Yuan, A novel polymeric precursor for micro/mesoporous nitrogen-doped carbons, *J. Mater. Chem. A* 1 (2013) 5113-5120.
- [43] K. Grygiel, PhD thesis "Poly(ionic liquid) stabilizers and new synthetic approaches", 2015, Uni Potsdam, Germany.
- [44] A. Silvestre-Albero, J. Silvestre-Albero, M. Martinez-Escandell, M. Molina-Sabio, A. Kovacs, F. Rodriguez-Reinoso, Novel synthesis of a micro-mesoporous nitrogen-doped nanostructured carbon from polyaniline, *Microp. Mesop. Mater.* 218 (2015) 199-205.
- [45] R. Ding, H. Wu, M. Thunga, N. Bowler, M.R. Kessler, Processing and characterization of low-cost electrospun carbon fibers from organosolv lignin/polyacrylonitrile blends, *Carbon* 100 (2016) 126-136.
- [46] J. Gong, J. Liu, X. Chen, Z. Jiang, X. Wen, E. Mijowska, T. Tang, Converting real-world mixed waste plastics into porous carbon nanosheets with excellent performance in the adsorption of an organic dye from wastewater, *J. Mater. Chem. A* 3 (2015) 341-351.
- [47] W. Shen, Y. He, S. Zhang, J. Li, W. Fan, Yeast-based microporous carbon materials for carbon dioxide capture, *ChemSusChem* 5 (2012) 1274-1279.
- [48] Y. Zhu, S. Murali, M.D. Stoller, K.J. Ganesh, W. Cai, P.J. Ferreira, A. Pirkle, R.M.

Wallace, K.A. Cychosz, M. Thommes, D. Su, E.A. Stach, R.S. Ruoff, Carbon-based supercapacitors produced by activation of graphene, *Science* 332 (2011) 1537-1541.

[49] P. Hu, D. Meng, G. Ren, R. Yan, X. Peng, Nitrogen-doped mesoporous carbon thin film for binder-free supercapacitor, *Appl. Mater. Today* 5 (2016) 1-8.

[50] G.-P. Hao, W.-C. Li, D. Qian, A.-H. Lu, Rapid synthesis of nitrogen-doped porous carbon monolith for CO₂ capture, *Adv. Mater.* 22 (2010) 853-857.

[51] M.C. Gutiérrez, D. Carriazo, C.O. Ania, J.B. Parra, M.L. Ferrer, F. del Monte, Deep eutectic solvents as both precursors and structure directing agents in the synthesis of nitrogen doped hierarchical carbons highly suitable for CO₂ capture, *Energy Environ. Sci.* 4 (2011) 3535-3544.

[52] S. Gadipelli, Z.X. Guo, Tuning of ZIF-derived carbon with high activity, nitrogen functionality, and yield-a case for superior CO₂ capture, *ChemSusChem* 8 (2015) 2123-2132.

[53] Y. Zhao, X. Liu, K.X. Yao, L. Zhao, Y. Han, Superior capture of CO₂ achieved by introducing extra-framework cations into N-doped microporous carbon, *Chem. Mater.* 24 (2012) 4725-4734.

[54] W. Xing, C. Liu, Z. Zhou, L. Zhang, J. Zhou, S. Zhuo, Z. Yan, H. Gao, G. Wang, S.Z. Qiao, Superior CO₂ uptake of N-doped activated carbon through hydrogen-bonding interaction, *Energy Environ. Sci.* 5 (2012) 7323-7327.

[55] X. Zhu, P.C. Hillesheim, S.M. Mahurin, C. Wang, C. Tian, S. Brown, H. Luo, G.M. Veith, K.S. Han, E.W. Hagaman, H. Liu, S. Dai, Efficient CO₂ capture by porous, nitrogen-doped carbonaceous adsorbents derived from task-specific ionic liquids, *ChemSusChem* 5 (2012) 1912-1917.

[56] Q.B. Meng, J. Weber, Lignin-based microporous materials as selective adsorbents for carbon dioxide separation, *ChemSusChem* 7 (2014) 3312-3318.

[57] Y. Luo, B. Li, W. Wang, K. Wu, B. Tan, Hypercrosslinked aromatic heterocyclic microporous polymers: A new class of highly selective CO₂ capturing materials, *Adv. Mater.* 24 (2012) 5703-5707.

[58] S.J. Yang, M. Antonietti, N. Fechner, Self-assembly of metal phenolic mesocrystals and morphosynthetic transformation toward hierarchically porous carbons, *J. Am. Chem. Soc.*

137 (2015) 8269-8273.

[59] S.M. Mahurin, P.F. Fulvio, P.C. Hillesheim, K.M. Nelson, G.M. Veith, S. Dai, Directed synthesis of nanoporous carbons from task-specific ionic liquid precursors for the adsorption of CO₂, *ChemSusChem* 7 (2014) 3284-3289.

[60] G.-P. Hao, Z.-Y. Jin, Q. Sun, X.-Q. Zhang, J.-T. Zhang, A.-H. Lu, Porous carbon nanosheets with precisely tunable thickness and selective CO₂ adsorption properties, *Energy Environ. Sci.* 6 (2013) 3740-3747.

[61] L.-L. Tan, H. Li, Y. Tao, S.X.-A. Zhang, B. Wang, Y.-W. Yang, Pillar[5]arene-based supramolecular organic frameworks for highly selective CO₂-capture at ambient conditions, *Adv. Mater.* 26 (2014) 7027-7031.

[62] G.-P. Hao, W.-C. Li, D. Qian, G.-H. Wang, W.-P. Zhang, T. Zhang, A.-Q. Wang, F. Schüth, H.-J. Bongard, A.-H. Lu, Structurally designed synthesis of mechanically stable poly(benzoxazine-*co*-resol)-based porous carbon monoliths and their application as high-performance CO₂ capture sorbents, *J. Am. Chem. Soc.* 133 (2011) 11378-11388.

[63] Z.-R. Jiang, H. Wang, Y. Hu, J. Lu, H.-L. Jiang, Polar group and defect engineering in a metal-organic framework: Synergistic promotion of carbon dioxide sorption and conversion, *ChemSusChem* 8 (2015) 878-885.

[64] J. Chen, J. Yang, G. Hu, X. Hu, Z. Li, S. Shen, M. Radosz, M. Fan, Enhanced CO₂ capture capacity of nitrogen-doped biomass-derived porous carbons, *ACS Sustainable Chem. Eng.* 4 (2016) 1439-1445.

[65] G. Sethia, A. Sayari, Comprehensive study of ultra-microporous nitrogen-doped activated carbon for CO₂ capture, *Carbon* 93 (2015) 68-80.

[66] W. Li, Y. Gao, W. Chen, P. Tang, W. Li, Z. Shi, D. Su, J. Wang, D. Ma, Catalytic epoxidation reaction over N-containing sp² carbon catalysts, *ACS Catal.* 4 (2014) 1261-1266.

[67] M.A. Patel, F. Luo, M.R. Khoshi, E. Rabie, Q. Zhang, C.R. Flach, R. Mendelsohn, E. Garfunkel, M. Szostak, H. He, P-doped porous carbon as metal free catalysts for selective aerobic oxidation with an unexpected mechanism, *ACS Nano* 10 (2016) 2305-2315.

[68] D.R. Dreyer, H.-P. Jia, C.W. Bielawski, Graphene oxide: A convenient carbocatalyst for facilitating oxidation and hydration reactions, *Angew. Chem. Int. Ed.* 49 (2010) 6813-6816.

[69] Y. Meng, D. Voiry, A. Goswami, X. Zou, X. Huang, M. Chhowalla, Z. Liu, T. Asefa, N-, O-, and S-tridoped nanoporous carbons as selective catalysts for oxygen reduction and alcohol oxidation reactions, *J. Am. Chem. Soc.* 136 (2014) 13554-13557.

Supplementary Material (SM) for

Main-chain poly(ionic liquid)-derived nitrogen-doped micro/mesoporous carbons for CO₂ capture and selective aerobic oxidation of alcohols

Jiang Gong ^a, Huijuan Lin ^a, Konrad Grygiel ^a, Jiayin Yuan ^{a,b,*}

^a Department of Colloid Chemistry, Max Planck Institute of Colloids and Interfaces, Research Campus Golm, D-14476, Potsdam, Germany

^b Department of Chemistry and Biomolecular Science, and Center for Advanced Materials Processing, Clarkson University, 8 Clarkson Avenue, 13699 Potsdam, USA

*Corresponding author. E-mail address: jiayin.yuan@mpikg.mpg.de; jyuan@clarkson.edu

Table S1 Comparison of the yield of nitrogen-doped carbons derived from different precursors according to the previously reported work.

Entry	Precursor	Temperature (°C)	Yield (wt %)	Ref. in <i>SM</i>
1	Poly(ionic liquid) (PIL)	1000	29.7	[S1]
2	PIL	1000	29	[S2]
3	PIL	1000	30	[S3]
4	PIL	1000	20	[S4]
5	PIL	800	24	[S4]
6	PIL	1000	21.4	[S5]
7	PIL	800	20.6	[S5]
8	PIL	750	30	[S6]
9	Ionic liquid (IL)	800	9.5–53	[S7]
10	IL	800	44.2	[S8]
11	IL	1000	21.8	[S9]
12	IL	1000	10	[S10]
13	Protic salts	1000	46	[S11]
14	Protic salts	100	36.5	[S12]
15	Protic salts	900	36.1	[S13]
16	Protic salts	1000	13	[S14]
17	Protic salts	800	23.3	[S15]
18	Polybenzoxazine	800	50–61	[S16]
19	Polyaniline	800	45	[S17]
20	Polypyrrole	800	35	[S18]
21	Polyacrylonitrile	1000	29.2	[S19]
22	PILPhDCA	600	73	This work
23	PILPhDCA	800	68	This work
24	PILPhDCA	900	66	This work
25	PILPhDCA	1000	64	This work

Table S2 Element composition of NPCs.

Entry	Sample	C ^a (wt %)	N ^a (wt %)	H ^a (wt %)	O ^b (wt %)
1	NPC-0	80.7	10.7	1.6	7.0
2	NPC-2	82.0	7.2	1.7	9.1
3	NPC-4	80.9	5.4	1.9	12.2
4	NPC-6	79.6	3.7	2.0	14.9

^a Measured by combustion element analyses. ^b Calculated by the difference.

Table S3 Surface element composition of NPCs measured by using XPS.

Entry	Sample	C (at %)	O (at %)	N (at %)	Pyridinic N (%)	Pyrrolic N (%)	Graphitic N (%)	Oxidized N (%)
1	NPC-0	79.8	8.1	12.1	48.2	20.6	26.7	4.5
2	NPC-2	81.8	9.9	8.3	38.9	20.9	35.8	4.5
3	NPC-4	80.1	13.7	6.2	33.7	25.4	33.4	7.5
4	NPC-6	79.7	15.8	4.5	46.7	17.8	23.8	12.2

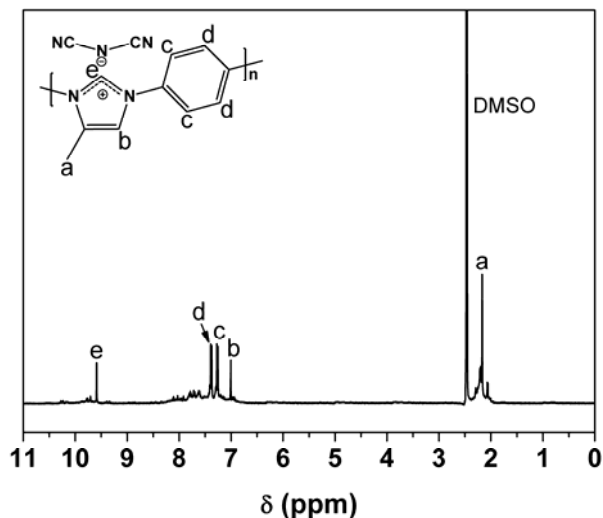


Fig. S1. ^1H NMR spectrum of PILPhDCA using $\text{DMSO-}d_6$ as the solvent.

The proton signals of $>\text{C-CH}_3$, $>\text{C=CH-N}<$, and $>\text{N=CH-N}<$ in the imidazole ring appear at 2.2, 7.0 and 9.6 ppm, respectively, while the phenyl protons show signals at 7.3 and 7.4 ppm, respectively.

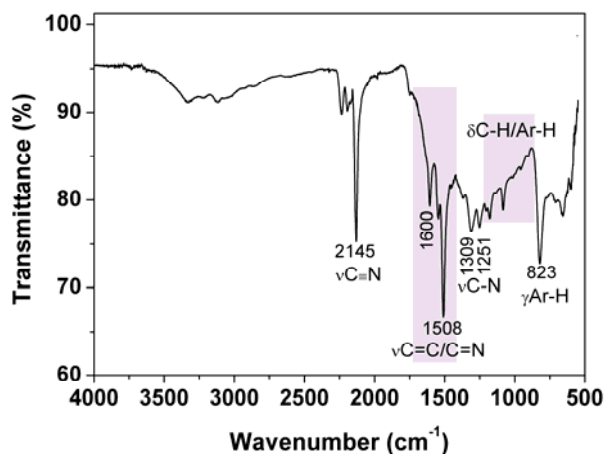


Fig. S2. FTIR spectrum of PILPhDCA.

The band at 2145 cm^{-1} is assigned to the $\text{C}\equiv\text{N}$ stretching vibration. Strong absorptions due to $\text{C}=\text{C}/\text{C}=\text{N}$ stretching vibrations found at 1508 and 1600 cm^{-1} reveal the presence of imidazole ring, which is confirmed by the imidazole ring-breathing mode at around 1251 and 1309 cm^{-1} . The in-plane C-H deformation of both benzene ring and imidazole ring is found in the region of $900\text{--}1200\text{ cm}^{-1}$. Additionally, in the range of $800\text{--}900\text{ cm}^{-1}$ we can clearly observe the out-of-plane deformation of the substituted benzene rings.

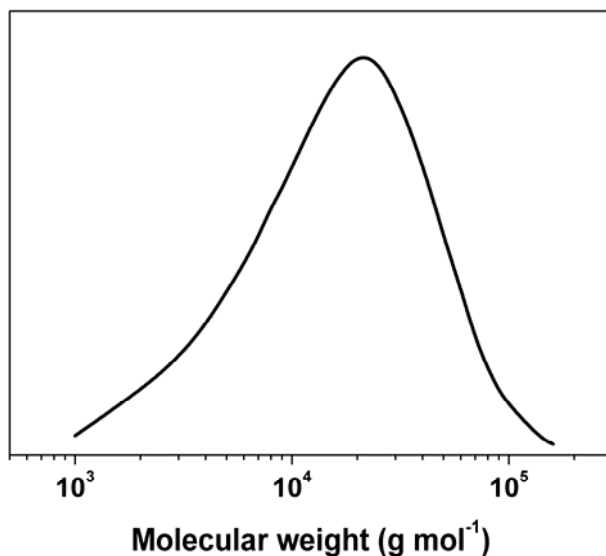


Fig. S3. GPC curve of PILPhAc.

Generally, GPC measurement indicates that the polymeric structures are successfully obtained during the performed reactions. The polymeric nature of the dialyzed PILPhAc was thus investigated by GPC. The synthesis of PILPhAc was halted at the early stage to access the product which retains soluble in water. The apparent number-average molecular weight of such PILPhAc can still reach $2 \times 10^4 \text{ g mol}^{-1}$. PILPhDCA was obtained by anion exchange from PILPhAc with excessive $\text{NaN}(\text{CN})_2$ in aqueous solution. In this case, the apparent number-average molecular weight of such PILPhDCA is determined to be ca. $2.1 \times 10^4 \text{ g mol}^{-1}$. It should be pointed out that the apparent number-average molecular weight of PILPhDCA for the preparation of NPCs is higher than $2.1 \times 10^4 \text{ g mol}^{-1}$, since the real synthesis of PILPhAc was not halted at early stage but to a full end of the reaction.

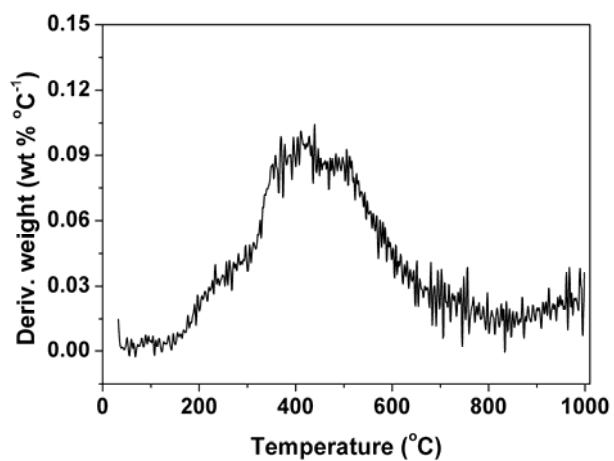


Fig. S4. DTG (the first derivative of TGA curve) curve for PILPhDCA under nitrogen atmosphere at 10 °C min⁻¹. As we can see, the temperature of the maximum weight loss rate is in the range of 360–510 °C.



Fig. S5. Photograph of the product NPC-4 synthesized on a large scale of as much as ~40 g.

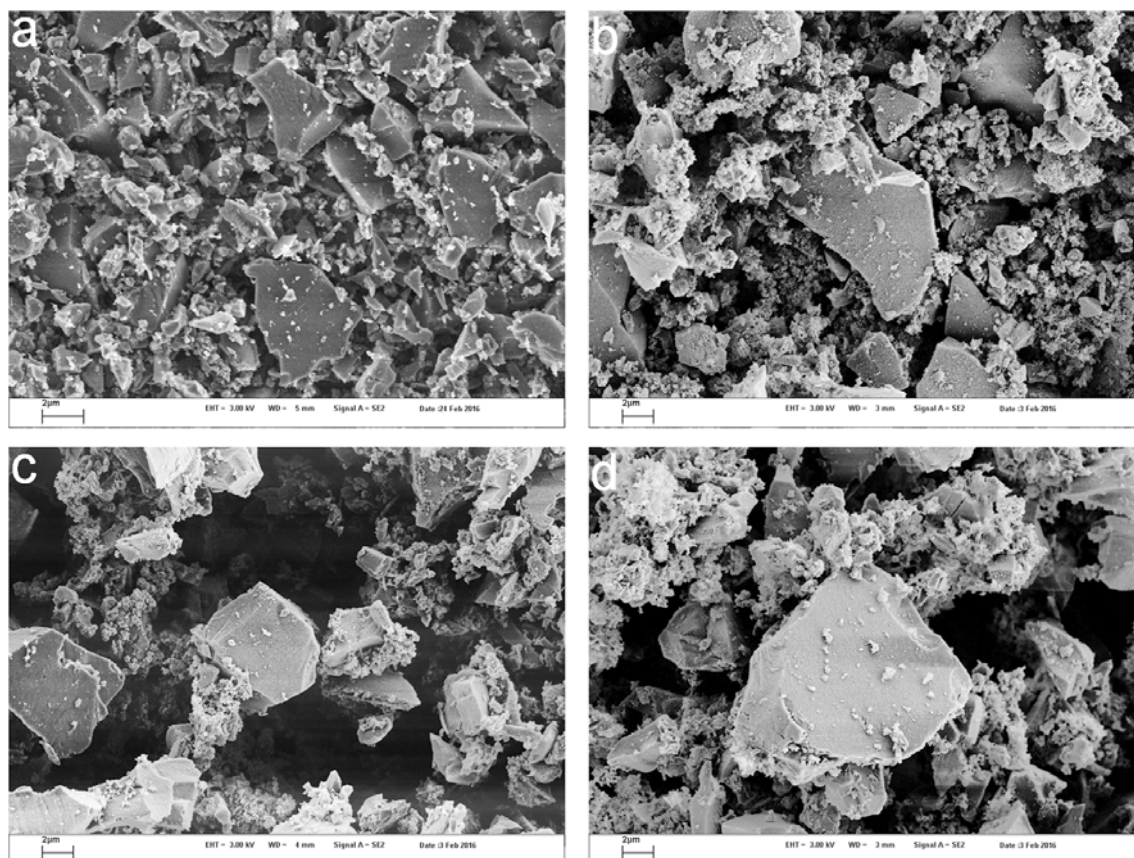


Fig. S6. Typical SEM images of (a) NPC-0, (b) NPC-2, (c) NPC-4, and (d) NPC-6 at a low magnification.

As we can see, NPCs comprise of many particles with a size ranging from several hundred nanometers to a couple of micrometers. In the SEM images at a low magnification, the activated samples show no obvious differences compared to the non-activated sample. This is possibly because during KOH activation the molten KOH firstly mixes well with the PIL-derived carbon and then produces micropores, which is hardly visible by SEM but easily confirmed by N_2 sorption measurements.

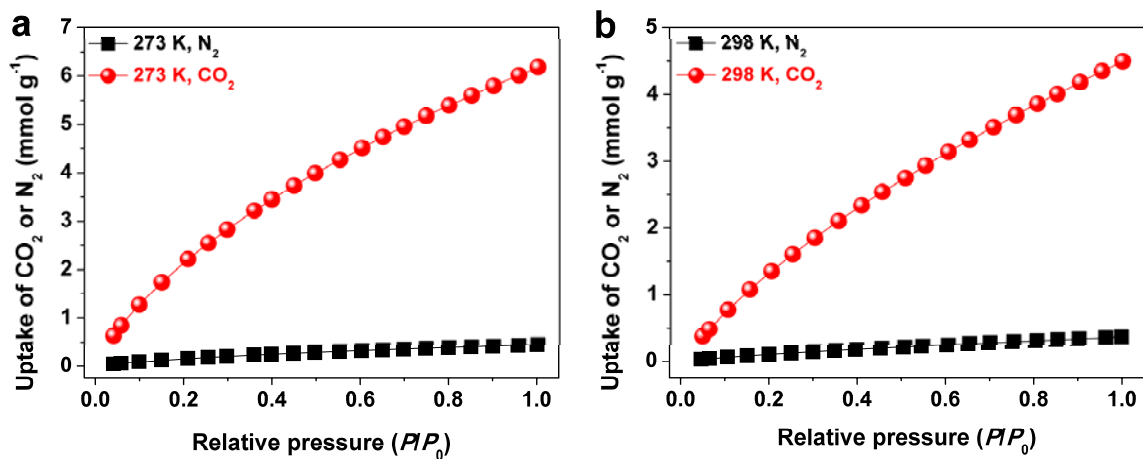


Fig. S7. CO₂ and N₂ adsorption isotherms of NPC-4 measured at (a) 273 K and (b) 298 K.

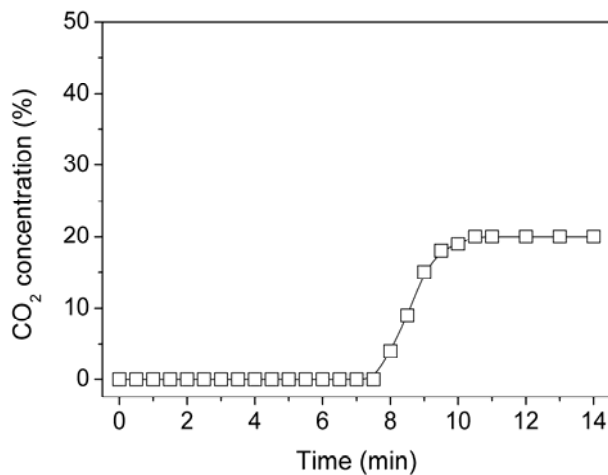


Fig. S8. Breakthrough curve for NPC-4 obtained at 298 K and 1 bar.

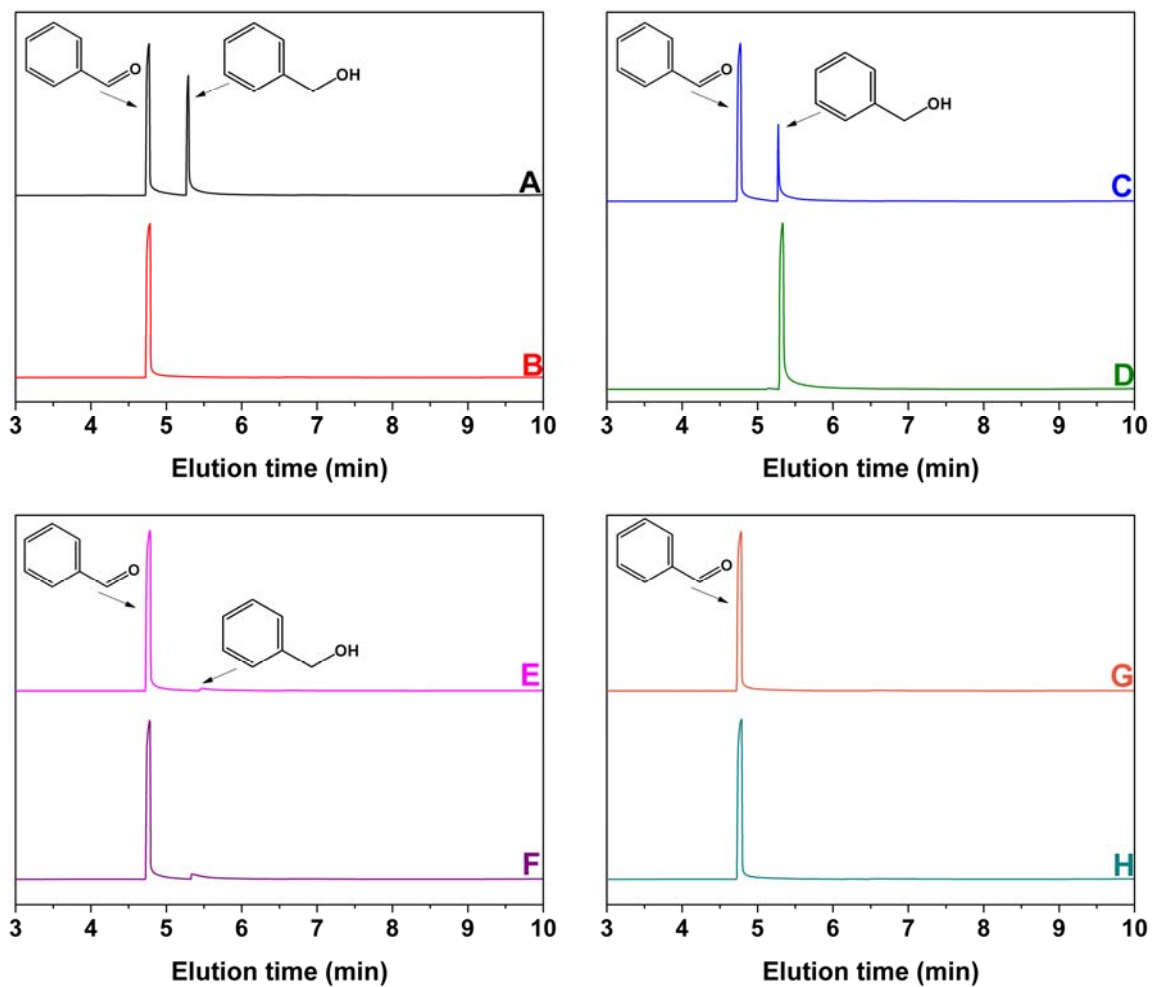


Fig. S9. GC-MS profiles of the product mixture from (A) entry 1, (B) entry 2, (C) entry 3, (D) entry 4, (E) entry 5, (F) entry 6, (G) entry 7, and (H) entry 8 in Table 3.

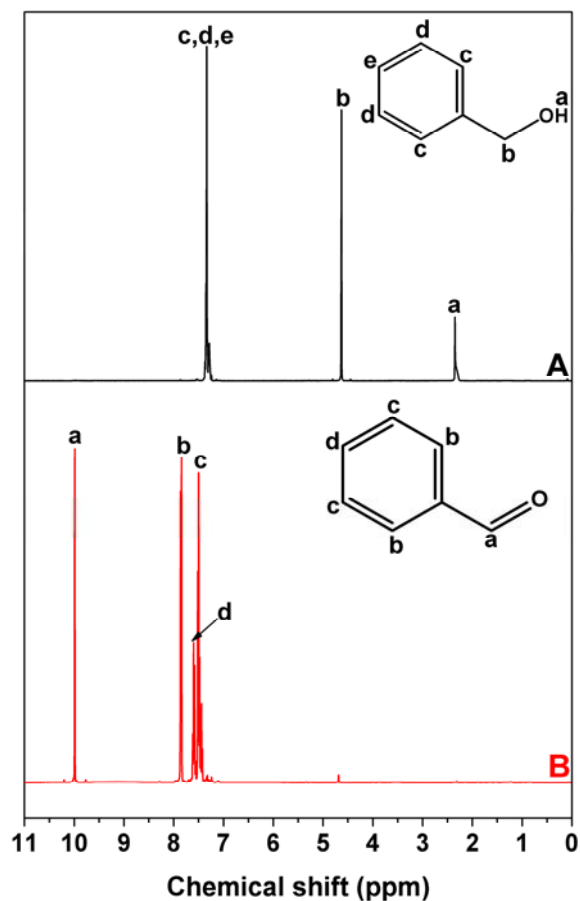


Fig. S10. ¹H NMR spectra of (A) benzyl alcohol and (B) the product from entry 2 in Table 3.

References to SM

[S1] J. Yuan, C. Giordano, M. Antonietti, Ionic liquid monomers and polymers as precursors of highly conductive, mesoporous, graphitic carbon nanostructures, *Chem. Mater.* 22 (2010) 5003-5012.

[S2] Q. Zhao, T.-P. Fellingner, M. Antonietti, J. Yuan, Nitrogen-doped carbon capsules *via* poly(ionic liquid)-based layer-by-layer assembly, *Macromol. Rapid Comm.* 33 (2012) 1149-1153.

[S3] S. Soll, T.-P. Fellingner, X. Wang, Q. Zhao, M. Antonietti, J. Yuan, Water dispersible, highly graphitic and nitrogen-doped carbon nanobubbles, *small* 9 (2013) 4135-4141.

[S4] Q. Zhao, T.-P. Fellingner, M. Antonietti, J. Yuan, A novel polymeric precursor for micro/mesoporous nitrogen-doped carbons, *J. Mater. Chem. A* 1 (2013) 5113-5120.

- [S5] M. Ambroggi, K. Sakaushi, M. Antonietti, J. Yuan, Poly(ionic liquid)s for enhanced activation of cotton to generate simple and cheap fibrous electrodes for energy applications, *Polymer* 68 (2015) 315-320.
- [S6] J. Gong, H. Lin, M. Antonietti, J. Yuan, Nitrogen-doped porous carbon nanosheets derived from poly(ionic liquid): Hierarchical pore structures for efficient CO₂ capture and dye removal, *J. Mater. Chem. A* 4 (2016) 7313-7321.
- [S7] J.S. Lee, X. Wang, H. Luo, G.A. Baker, S. Dai, Facile ionothermal synthesis of microporous and mesoporous carbons from task specific ionic liquids, *J. Am. Chem. Soc.* 131 (2009) 4596-4597.
- [S8] J.S. Lee, X. Wang, H. Luo, S. Dai, Fluidic carbon precursors for formation of functional carbon under ambient pressure based on ionic liquids, *Adv. Mater.* 22 (2010) 1004-1007.
- [S9] J.P. Paraknowitsch, J. Zhang, D. Su, A. Thomas, M. Antonietti, Ionic liquids as precursors for nitrogen-doped graphitic carbon, *Adv. Mater.* 22 (2010) 87-92.
- [S10] J.P. Paraknowitsch, B. Wienert, Y. Zhang, A. Thomas, Intrinsically sulfur- and nitrogen-co-doped carbons from thiazolium salts, *Chem. Eur. J.* 18 (2012) 15416-15423.
- [S11] S. Zhang, K. Dokko, M. Watanabe, Direct synthesis of nitrogen-doped carbon materials from protic ionic liquids and protic salts: Structural and physicochemical correlations between precursor and carbon, *Chem. Mater.* 26 (2014) 2915-2926.
- [S12] S. Zhang, M.S. Miran, A. Ikoma, K. Dokko, M. Watanabe, Protic ionic liquids and salts as versatile carbon precursors, *J. Am. Chem. Soc.* 136 (2014) 1690-1693.
- [S13] S. Zhang, A. Ikoma, K. Ueno, Z. Chen, K. Dokko, M. Watanabe, Protic-salt-derived nitrogen/sulfur-codoped mesoporous carbon for the oxygen reduction reaction and supercapacitors, *ChemSusChem* 8 (2015) 1608-1617.
- [S14] S. Zhang, H.-M. Kwon, Z. Li, A. Ikoma, K. Dokko, M. Watanabe, Nitrogen-doped inverse opal carbons derived from an ionic liquid precursor for the oxygen reduction reaction, *ChemElectroChem* 2 (2015) 1080-1085.
- [S15] S. Zhang, T. Mandai, K. Ueno, K. Dokko, M. Watanabe, Hydrogen-bonding supramolecular protic salt as an "all-in-one" precursor for nitrogen-doped mesoporous carbons for CO₂ adsorption, *Nano Energy* 13 (2015) 376-386.

- [S16] S. Mahadik-Khanolkar, S. Donthula, C. Sotiriou-Leventis, N. Leventis, Polybenzoxazine aerogels. 1. High-yield room-temperature acid-catalyzed synthesis of robust monoliths, oxidative aromatization, and conversion to microporous carbons, *Chem. Mater.* 26 (2014) 1303-1317.
- [S17] A. Silvestre-Albero, J. Silvestre-Albero, M. Martinez-Escandell, M. Molina-Sabio, A. Kovacs, F. Rodriguez-Reinoso, Novel synthesis of a micro-mesoporous nitrogen-doped nanostructured carbon from polyaniline, *Microp. Mesop. Mater.* 218 (2015) 199-205.
- [S18] J.W.F. To, J. He, J. Mei, R. Haghpanah, Z. Chen, T. Kurosawa, S. Chen, W.-G. Bae, L. Pan, J.B.-H. Tok, J. Wilcox, Z. Bao, Hierarchical N-doped carbon as CO₂ adsorbent with high CO₂ selectivity from rationally designed polypyrrole precursor, *J. Am. Chem. Soc.* 138 (2016) 1001-1009.
- [S19] R. Ding, H. Wu, M. Thunga, N. Bowler, M.R. Kessler, Processing and characterization of low-cost electrospun carbon fibers from organosolv lignin/polyacrylonitrile blends, *Carbon* 100 (2016) 126-136.